

Article

Determination of Transport Pathways and Mutual Exchanges of Atmospheric Moisture between Source Regions of Yangtze and Yellow River Basins

Beiming Kang^{1,2,3,4}, Jiahua Wei^{1,2,3,4,5,*} , Olusola O. Ayantobo⁶  and Haijiao Yang^{1,2,3,4}

- ¹ School of Civil Engineering and Water Resources, Qinghai University, Xining 810016, China; 2014990028@qhu.edu.cn (B.K.); 2014990031@qhu.edu.cn (H.Y.)
- ² State Key Laboratory of Plateau Ecology and Agriculture, Qinghai University, Xining 810016, China
- ³ Laboratory of Ecological Protection and High-Quality Development in the Upper Yellow River, Qinghai University, Xining 810016, China
- ⁴ Key Laboratory of Water Ecology Remediation and Protection at Headwater Regions of Big Rivers, Ministry of Water Resources, Xining 810016, China
- ⁵ State Key Laboratory of Hydrosience and Engineering, Tsinghua University, Beijing 100084, China
- ⁶ College of Civil Engineering and Architecture, Guangxi University, Nanning 530004, China; skollar24k@yahoo.com
- * Correspondence: weijiahua@tsinghua.edu.cn

Abstract: Knowledge of the quantitative importance of the moisture transport pathways and mutual moisture exchange of the source regions of the Yangtze (SYZR) and Yellow (SYR) rivers' basins, the adjacent origins of China's two longest rivers, can provide insights into the regional atmospheric branch of the hydrological cycle over the source regions. The method with the Hybrid Single-Particle Lagrangian Integrated Trajectory (HYSPLIT) model and a Lagrangian moisture source diagnostic to identify the major moisture transport pathways quantifies their importance to two types of daily precipitation events—daily precipitation more than 10 mm (PM) events and daily precipitation less than 10 mm (PL) events—for the two rivers' regions during the summer (June–August, 1986–2015) and finds the characteristics of mutual moisture exchange. The results indicated that both the Bay of Bengal group pathway and the northwest China group pathway play significant roles in PM and PL events over the SYZR, contributing 41.87% and 39.12% to PM events and 41.33% and 33.16% to PL events, respectively. The SYR has five main moisture path groups; the Bay of Bengal group pathway, the northwest China group pathway, and the southeast China group pathway play significant roles in PM and PL events over the SYR, contributing 32.34%, 23.28%, and 34.36% to PM events and 34.84%, 36.18%, and 19.83% to PL events, respectively. The volume of moisture passing from the SYZR to the SYR is approximately 60 times that of the reverse, constituting about 6.9% of the total moisture released in SYR precipitation. It is worth noting that the moisture release was concentrated in the nearer west group pathway, and the main moisture uptake locations were beyond the source region of the two rivers (remote sources) in the PM events. The aggregate moisture release high-frequency moisture transport path groups are found in the southeastern parts of Zhiduo County and the southeast of Zaduo County.

Keywords: moisture pathways; moisture exchange; Lagrangian trajectory model; source regions of the Yangtze and Yellow River



Citation: Kang, B.; Wei, J.; Ayantobo, O.O.; Yang, H. Determination of Transport Pathways and Mutual Exchanges of Atmospheric Moisture between Source Regions of Yangtze and Yellow River Basins. *Atmosphere* **2024**, *15*, 524. <https://doi.org/10.3390/atmos15050524>

Academic Editor: Yoshihiro Tomikawa

Received: 6 April 2024
Accepted: 18 April 2024
Published: 25 April 2024



Copyright: © 2024 by the authors. Licensee MDPI, Basel, Switzerland. This article is an open access article distributed under the terms and conditions of the Creative Commons Attribution (CC BY) license (<https://creativecommons.org/licenses/by/4.0/>).

1. Introduction

The Yangtze and Yellow Rivers are China's two longest rivers, with both originating from the eastern part of the Tibetan Plateau (TP) and their source regions lying adjacent to each other [1,2]. These source regions constitute vital ecological barriers in Asia, playing a pivotal role in the intricate dynamics of the global water cycle, hydrological equilibrium, and the provisioning of water resources. Approximately 40% of the Yellow River's total

runoff and 1.3% of the Yangtze River's total runoff originate from these regions [3–5]. With the warming and humid climate trends over the TP, these source regions are increasingly contributing to river runoff. The average annual precipitation in the SYR is about 502.72 mm, while the SYZR, being colder and drier, receives an average of 343.89 mm of precipitation annually, indicating a significant disparity between the two source regions [6]. As the atmospheric moisture transport process is an important part of the hydrological cycle, the knowledge of where moisture comes from (moisture sources), how it is transported (moisture transport pathways), and how it is exchanged (mutual moisture exchange) is of great value to provide a full picture of the hydrological cycle in the SYZR and the SYR, and this issue deserves a systematic and in-depth study.

A considerable amount of research has been conducted on the atmospheric moisture transport characteristics of precipitation in both the two river source regions and the TP [7]. Previous studies predominantly employed the Eulerian method; however, in recent years, there has been an increasing trend towards utilizing the Lagrangian approach [8,9]. Research primarily focuses on two aspects: atmospheric moisture transport pathways and the contribution of different atmospheric moisture pathways to regional rainfall [10,11]. During summer and autumn, the TP primarily experiences two moisture pathways originating from the Indian Ocean and the Eurasian continent, while during spring and winter, the mid-latitude westerlies serve as the main moisture source pathways for the TP [12]. Due to variations in study areas, seasons, and rainfall intensity, different atmospheric moisture transport pathways exhibit significant differences in their contribution to regional precipitation. Zhang et al. [13] utilized the HYSPLIT model to study the characteristics of moisture transport during the rainy season in the Three-River Headwaters Region (TRHR), identifying northwest and southern China pathways as the main contributors to extreme and moderate precipitation events in the region. The contribution rates of these pathways to the two types of precipitation events were found to be 18.4% and 25.9% for the northwest pathway and 32.2% and 28.5% for the southern China pathway, respectively. In extreme drought events, the far-western Asia pathway plays a dominant role. Xu et al. [12] observed that during the period from 1979 to 2018, the mid-latitude westerlies' contribution to precipitation in the TP increased, while the contribution from the southern Indian Ocean decreased. Tang et al.'s [14] study on moisture source variations in the TP from 1979 to 2013 found that land-sourced moisture accounted for 69%, while ocean-sourced moisture accounted for approximately 21%. Zhu et al. [15] revealed that the vast arid and semi-arid grassland areas north of the TP were the primary moisture sources for precipitation in the Yellow River source area in July 2015, with a contribution rate as high as 52.9%. However, this contribution rate significantly decreased in July 2012. Research on the characteristics of moisture transport in the source regions of the two rivers, which possess abundant atmospheric water resources [16], is scarce despite the inevitable mutual moisture exchange between neighboring river source regions. Research on the atmospheric moisture transport and exchange characteristics between the two river source regions aims to explore the feasibility of the cross-basin allocation of atmospheric moisture resources through artificial weather modification operations. This provides insights into addressing watershed water scarcity through the development of atmospheric moisture resources.

The details of the dataset and methodology are described in Section 2. The results are shown in Section 3. Discussions and the major conclusions are provided in Section 4.

2. Data and Methods

2.1. Study Area

The study area encompasses the SYZR and the SYR, situated in the eastern part of the TP, ranging from 32°12' N to 36°15' N and 90°23' E to 103°28' E. The respective regions are 142,714 km² and 122,971 km², with average elevations of 4757.42 m and 4127.06 m. The annual average temperatures are 0.16 °C and 0.86 °C, while the annual average precipitation is 343.89 mm and 502.72 mm. Approximately 80% of the precipitation occurs during the summer. Topographical maps of the two river source regions are presented in Figure 1.

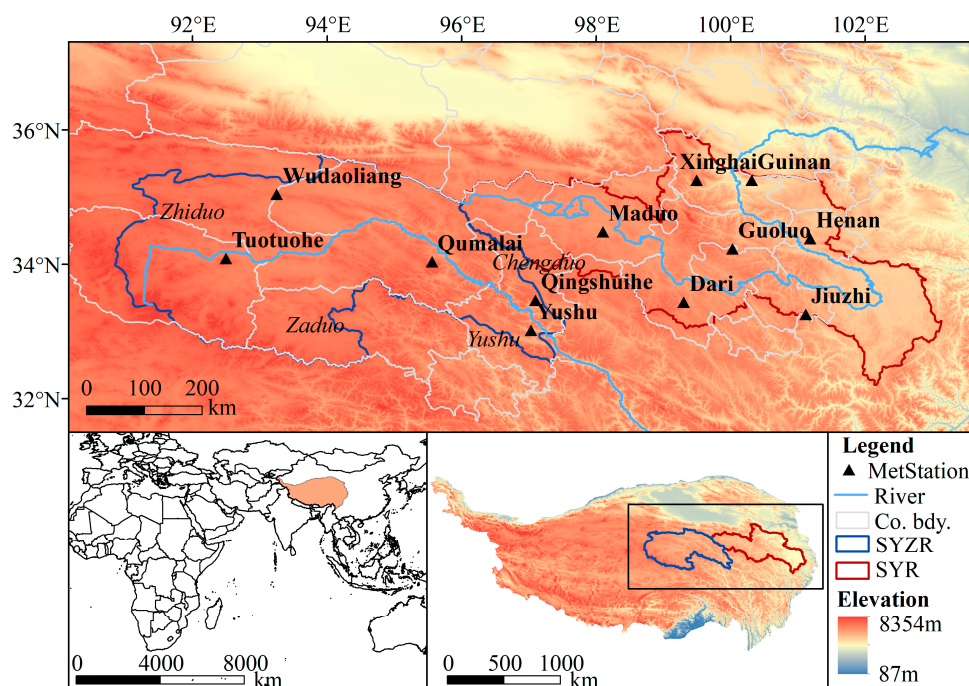


Figure 1. A topographical map of the two river source regions. Co. bdy. stands for the county boundary.

2.2. Definition of Two Types of Daily Precipitation Events

Summer (June–August) daily precipitation data (1986–2015) from 12 meteorological stations located inside the study area (Figure 1) are used to define two types of daily precipitation events. The daily precipitation data are provided by the China National Meteorological Information Center [17]. First, precipitation intensity is classified according to the 24 h precipitation amount categories adopted by the Chinese Meteorological Department [18] (Table 1). The proportion of rainstorms and above precipitation is 0.30%; heavy precipitation accounts for 6.96%, moderate precipitation for 39.38%, and light precipitation for 53.37%.

Table 1. Classification of precipitation types for 24 h.

Grade	Extra Heavy Rainstorm	Heavy Rainstorm	Rainstorm	Heavy Precipitation	Moderate Precipitation	Light Precipitation
24 h Precipitation Amount (mm)	≥250	100–249.9	50–99.9	25–49.9	10–24.9	0.1–9.9
Proportion (%)		0.30		6.96	39.38	53.37

According to the precipitation proportion, precipitation events can be roughly divided into two types: daily precipitation less than 10 mm (PL) events and daily precipitation more than 10 mm (PM) events. Due to the extremely harsh climatic conditions in the study area and the sparse distribution of meteorological stations, gridded daily precipitation data (0.25° × 0.25°) from the Asian Precipitation-Highly Resolved Observational Data Integration Toward Evaluation of Water Resources [APHRODITE; versions APHRO_MA_V1101 (1960–2007) and APHRO_MA_V1101_EX_R1 (2008–15)] [19] project are used to depict the precipitation conditions of the corresponding precipitation events. Zhang’s research [13] indicates satisfactory consistency between the station data and the APHRODITE data in the spatial and temporal variability of the precipitation over the study area.

2.3. Trajectory Generation Description

The HYSPLIT model, developed by Draxler and Hess [20,21], is used to calculate air parcel trajectories and analyze complex transport phenomena. It has gradually been

applied in the study of moisture transport characteristics. The reprocessed NCEP data (HYSPLIT-compatible format) are used to drive the model; the data which are used include surface variables like pressure, temperature at 2 m, and wind components at 10 m, as well as upper-level atmospheric data across various pressure levels from 1000 to 10 hpa, covering heights, temperature, wind direction and speed, vertical wind speed, and relative humidity. Due to the distribution law of atmospheric moisture density, moisture density decreases rapidly with the increase in altitude, and moisture is mainly distributed in the atmosphere below 5 km [22], so a release grid ($0.75^\circ \times 0.75^\circ$) clipped by the regional boundary with 10 vertical levels is defined as the release positions of the trajectories [note a broad vertical range, 0–5 km above ground level (AGL) with an interval of 0.5 km]. The trajectory simulation runs backward in time for 240 h, which is the average residence time of moisture in the atmosphere [23,24]. To cover the entire duration of each precipitation event, the simulation for each trajectory commences at 0000 UTC on the second day following the onset of each precipitation event.

The latitude, longitude, height, pressure, specific humidity, and mixed-layer depth are selected as the output parameters, and the output time interval is 1 h. The total numbers of trajectories generated for the two precipitation types are shown in Table 2. In addition, not all trajectories bring moisture to the starting point of the trajectory, and only those that steadily release moisture in the starting point should be considered valid moisture trajectories. That is, moisture trajectories in the present study are defined as those that have statistically significant ($p < 0.05$) negative trends of moisture content in the target region [13].

Table 2. Description used to identify two types of precipitation events, number of generated trajectories, valid trajectories.

Region	No. of Grids	Event	Mean Precipitation Rate (mm/d)	No. of Events (Average Times/Grid Points)	No. of Traj.	No. of Valid Traj.
Source Region of Yangtze River (SYZR)	26	PM	14.51	48.04	12,560	4203
		PL	4.41	409.19	32,260	13,285
Source Region of Yellow River (SYR)	28	PM	15.25	127.13	29,190	7429
		PL	4.61	669.96	130,970	33,039

PM indicates the daily precipitation is greater than 10 mm events; PL indicates the daily precipitation is less than 10 mm events.

2.4. Trajectory Clustering Method

The HYSPLIT model's built-in clustering method is K-means, and it is incapable of clustering trajectories starting from different points [25]. In this study, trajectory files generated by the HYSPLIT model, with different starting points, are still clustered using the K-means method. The range of cluster numbers is determined by identifying the 'elbow' in the average deviation. Within this range, the silhouette coefficient is calculated, and the number of clusters corresponding to the maximum silhouette coefficient value is selected as the final number of clusters (K) [26], thereby achieving the clustering of trajectories with different starting points. As shown in Figure 2, the average deviation range of K at the 'elbow' is 3–6. When K equals 4, which corresponds to the highest silhouette coefficient value, it is selected as the optimal number of clusters.

Applying the previously mentioned method, the valid trajectories of the SYZR and SYR were clustered, with clustering numbers (N) of 4 and 5, respectively. The average deviation and silhouette coefficients for different clustering numbers are presented in Figure A1 and Table A1 (See Appendix A), respectively.

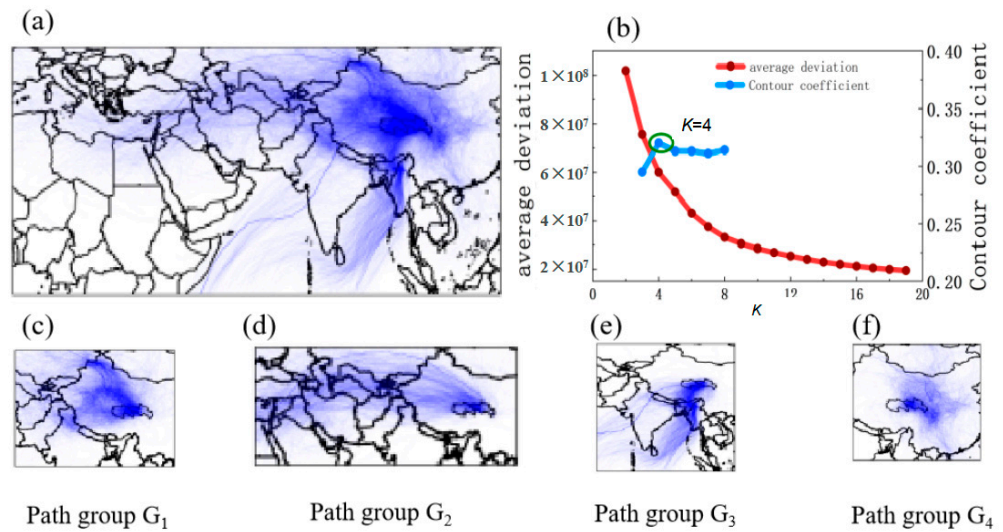


Figure 2. Workflow of trajectory clustering. The blue lines represent trajectories. (a) All moisture trajectories; (b) number of clusters is determined using average deviation and contour coefficients; K indicates the clustering number. (c–f) different path groups after clustering moisture trajectories, labeled as path group G_1 , path group G_2 , path group G_3 , and path group G_4 .

2.5. Method for Moisture Sources Attribution, Calculating Moisture Path Frequency, and Determining Average Path Humidity

The method for moisture sources’ attribution is based on the principles of the S08 and SW14 methods [27,28], which were employed to estimate the moisture contributions from each source region to the precipitation falling in the target area. The sketch of the method for moisture sources’ attribution is given in Figure 3.

- (1) Identify the moisture uptake and release locations along the moisture trajectory by calculating the moisture changes between neighboring time points. A threshold $e_c = 0.2 \text{ g}\cdot\text{kg}^{-1} (6 \text{ h})^{-1}$ is set to select the moisture uptake locations with a moisture uptake amount larger than e_c between the neighboring time points, as performed by Sodemann et al. [28].
- (2) Traverse the locations of moisture uptake, loss, and release forward in time. The initial values of the discounted moisture uptake amount Δq are set to $\Delta l_{-n,0}$.
- (3) Assume we are at time = $-6(n - 1)$, moisture uptake amounts between time = $-6n$ and time = $-6(n - 1)$ are $\Delta q_{-6(n - 1)}$. The moisture attribution rate by the current uptake location is $f_{-6(n - 1)}$. When at time = -12 , which is the moisture release time, the portion of the current released moisture amount that comes from the moisture uptake at time = $-6(n - 1)$ is $\Delta l_{-6(n - 1), -12}$, and the remaining amounts come from the moisture uptake at time = $-6(n - 1)$, denoted as $\Delta q_{-6(n - 1), -12}$; the current released moisture amount attribution rate that comes from the moisture uptake at time = $-6(n - 1)$ is $f_{-6(n - 1), -12}$. When at time = 0 , which is also a moisture release time, the portion of the current released moisture amount that comes from the moisture uptake at time = $-6(n - 1)$ is $\Delta l_{-6(n - 1), 0}$, and the remaining amounts come from the moisture uptake at time = $-6(n - 1)$, denoted as $\Delta q_{-6(n - 1), 0}$; the current released moisture amount attribution rate that comes from the moisture uptake at time = $-6(n - 1)$ is $f_{-6(n - 1), 0}$.

$$\Delta q_{-6(n-1)} = q_{-6(n-1)} - q_{-6n} \tag{1}$$

$$f_{-6(n-1)} = \frac{\Delta q_{-6(n-1)}}{q_{-6(n-1)}} \tag{2}$$

$$f_{-6(n-1),-18} = \frac{\Delta q_{-6(n-1)}}{q_{-18}} \tag{3}$$

$$\Delta l_{-6(n-1),-12} = \Delta l_{-12} \times f_{-6(n-1),-18} \tag{4}$$

$$\Delta q_{-6(n-1),-12} = \Delta q_{-6(n-1)} - \Delta l_{-6(n-1),-12} \tag{5}$$

$$f_{-6(n-1),-6} = \frac{\Delta q_{-6(n-1),-12}}{q_{-6}} \tag{6}$$

$$\Delta l_{-6(n-1),-0} = \Delta l_{-12} \times f_{-6(n-1),-6} \tag{7}$$

$$\Delta q_{-6(n-1),-0} = \Delta q_{-6(n-1)} - \Delta l_{-6(n-1),-12} - \Delta l_{-6(n-1),-0} \tag{8}$$

- (4) For this trajectory, the moisture sources' attribution from remote sources, the SYZR and SYR, is $\Delta l_{-6(n-1),0}$, $\Delta l_{-18,0}$, and $\Delta l_{-6,0}$, respectively. The contributions of different moisture sources can be obtained by accumulating the moisture source attributions of all trajectories for remote sources, the SYZR, and the SYR, denoted as $\Delta l_{\text{remote_sources}}$, Δl_{SYZR} , and Δl_{SYR} , respectively.
- (5) Calculate the total moisture release amount within the target region at time $t = 0$, denoted as R_{total} . The contribution rates of different moisture sources can be obtained by dividing the moisture source attributions of all trajectories from remote sources, the SYZR, and the SYR by R_{total} .

$$R_{\text{total}} = \sum_{i=1}^L \Delta q_{0,i} \tag{9}$$

where L is the total number of valid trajectories, and $\Delta q_{0,i}$ is the moisture release amounts between time = -6 and time = 0 of the i -th trajectory.

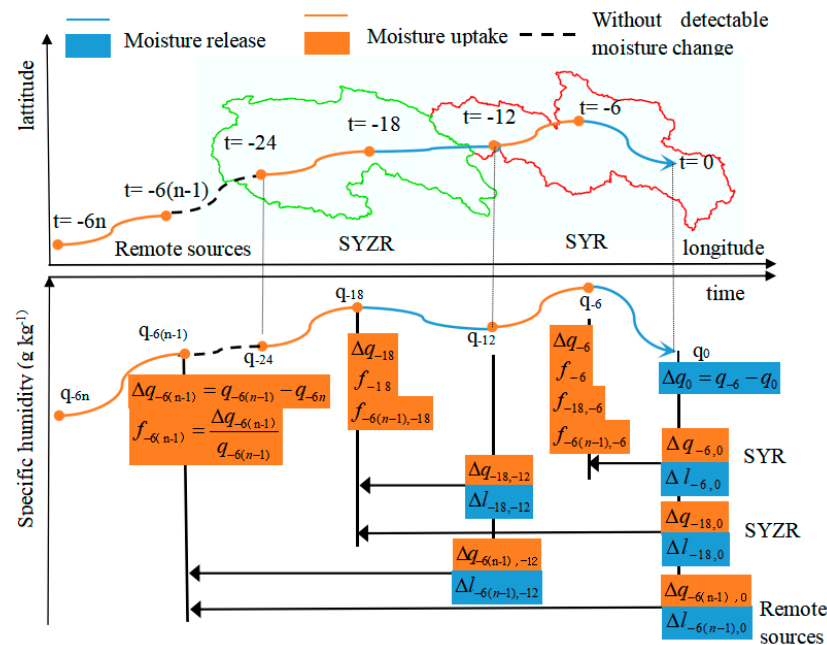


Figure 3. A sketch of the method for moisture sources' attribution. Time points $t = -6n$ and $-6(n - 1)$ are remote sources; time points $t = -24$ and -18 are SYZR sources; time points $t = -12$, -6 , and 0 are SYR sources. (**top**) The geographic location of the trajectory. Orange segments and orange lines indicate moisture uptake processes between the neighboring time points, blue segments and blue lines indicate moisture release processes between the neighboring time points, and black segments indicate moisture without detectable change between the neighboring time points. (**bottom**) The specific humidity changes along the trajectory. Orange blocks indicate moisture uptake amounts, and blue blocks indicate moisture release amounts that can be attributed to certain moisture uptake location.

The frequency of moisture trajectories passing over a grid cell (i, j) F_{ij} ($0.75^\circ \times 0.75^\circ$ grid) is calculated by Equation (10); a higher trajectory frequency indicates that moisture trajectories pass through the grid cell more frequently.

The average specific humidity of moisture trajectories gridded onto each grid cell is calculated by Equation (11). A higher average specific humidity indicates that the trajectories carry abundant moisture.

$$F_{ij} = \frac{M}{L} \quad (10)$$

$$\bar{q}_{ij} = \frac{q_{ij1} + q_{ij2} + \dots + q_{ijn}}{M} \quad (11)$$

where F_{ij} is the path frequency; L is the total number of valid trajectories; M is the number of paths passing through a grid cell (i, j) ; \bar{q}_{ij} is the average humidity at a grid cell (i, j) ; q_{ijn} is the specific humidity of the n -th trajectory passing through the grid cell (i, j) .

3. Results

3.1. Major Moisture Transport Path Groups

Figures 4 and 5 show the clustering results of moisture trajectories. In PM events of the SYZR (Figure 4a–d), there are four path groups. Path group1 (SYZR PM1, farther west group) started from a location much farther than West Asia and includes 400 valid trajectories. Path group2 (SYZR PM2, nearer west group) started from West Asia and is also controlled by the westerlies and includes 892 valid trajectories. Path group3 (SYZR PM3, Bay of Bengal group) started from the Bay of Bengal and Arabian Sea and includes 1580 valid trajectories. Path group4 (SYZR PM4, northwest China group) corresponds with the northwest of China and includes 1331 valid trajectories. In PL events of the SYZR (Figure 4e,f), there are also four path groups. Path group1 (SYZR PL1), path group2 (SYZR PL2), path group3 (SYZR PL3), and path group4 (SYZR PL4) contain 937, 6413, 2990, and 2945 valid trajectories, respectively, similar to the origin of the SYZR PM paths.

The PM events of the SYR (Figure 5a–e) have five path groups. Path group1 (SYR PM1) started from a location much farther west than West Asia and includes 343 valid trajectories. Path group2 (SYR PM2) started from West Asia and includes 1247 valid trajectories. Path group3 (SYR PM3) started from the Bay of Bengal and Arabian Sea and includes 1865 valid trajectories. Path group4 (SYR PM4) corresponds with the northwest of China and includes 2272 valid trajectories. Path group5 (SYR PM5, southeast China group) corresponds with the east of China and includes 1702 valid trajectories. The PL events of the SYR (Figure 5f–h) also have five path groups. The five path groups (SYR PL1, SYR PL2, SYR PL3, SYR PL4, SYR PL5) contain 1627, 4785, 9831, 8030, and 8766 valid trajectories, respectively, similar to the origin of the SYR PM paths.

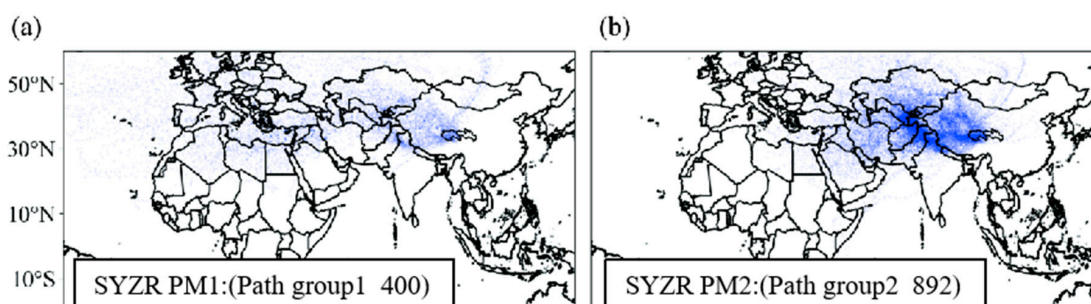


Figure 4. Cont.

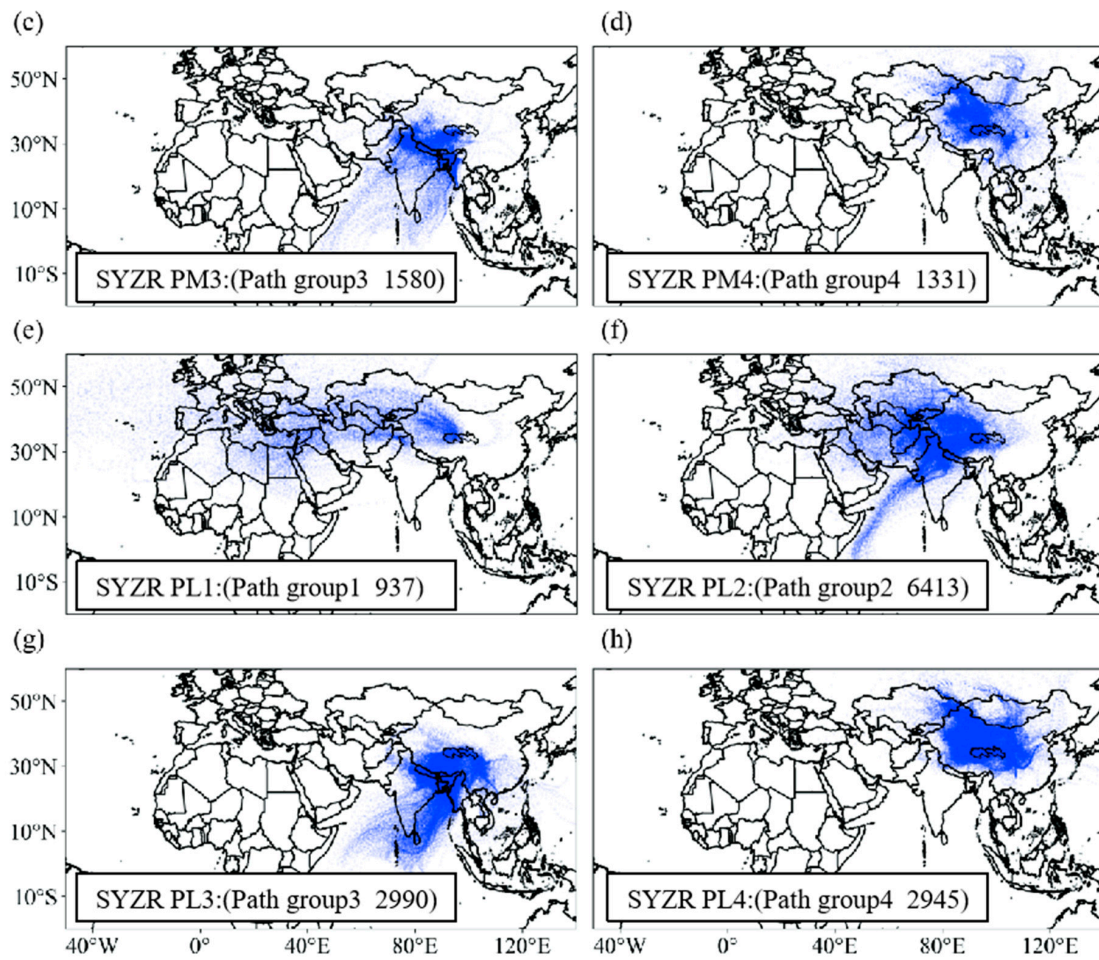


Figure 4. The clustering results of moisture trajectories for the SYZR. The blue lines represent trajectories. (a–d) are PM events; (e–h) are PL events. PM indicates the daily precipitation is greater than 10 mm events; PL indicates the daily precipitation is less than 10 mm events. SYR indicates the source regions of the Yellow River basin. SYZR indicates the source regions of the Yangtze River basin.

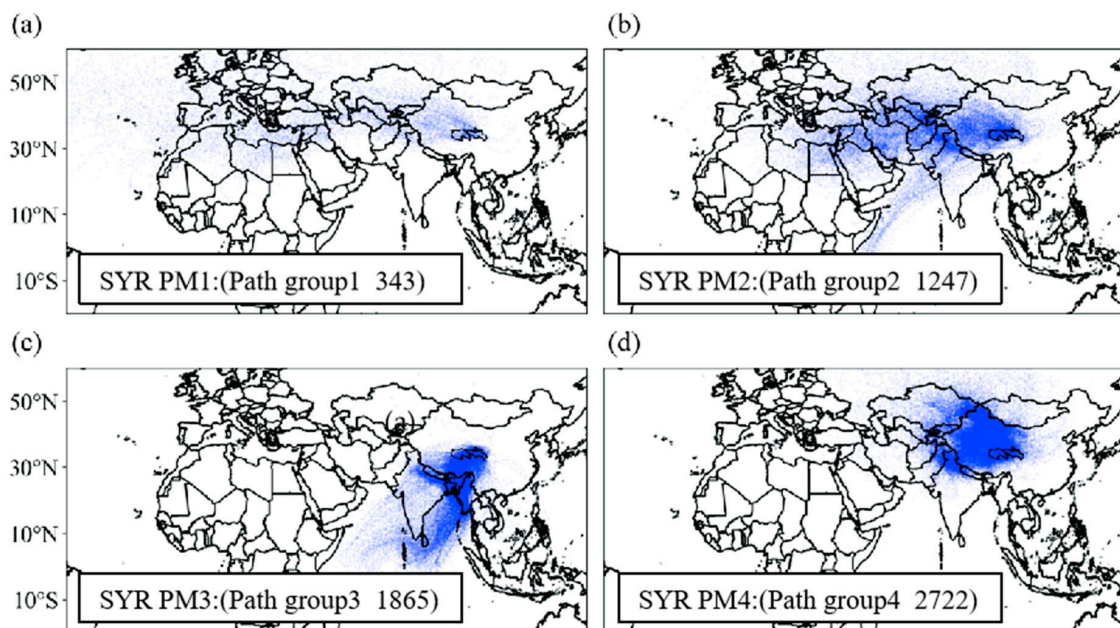


Figure 5. Cont.

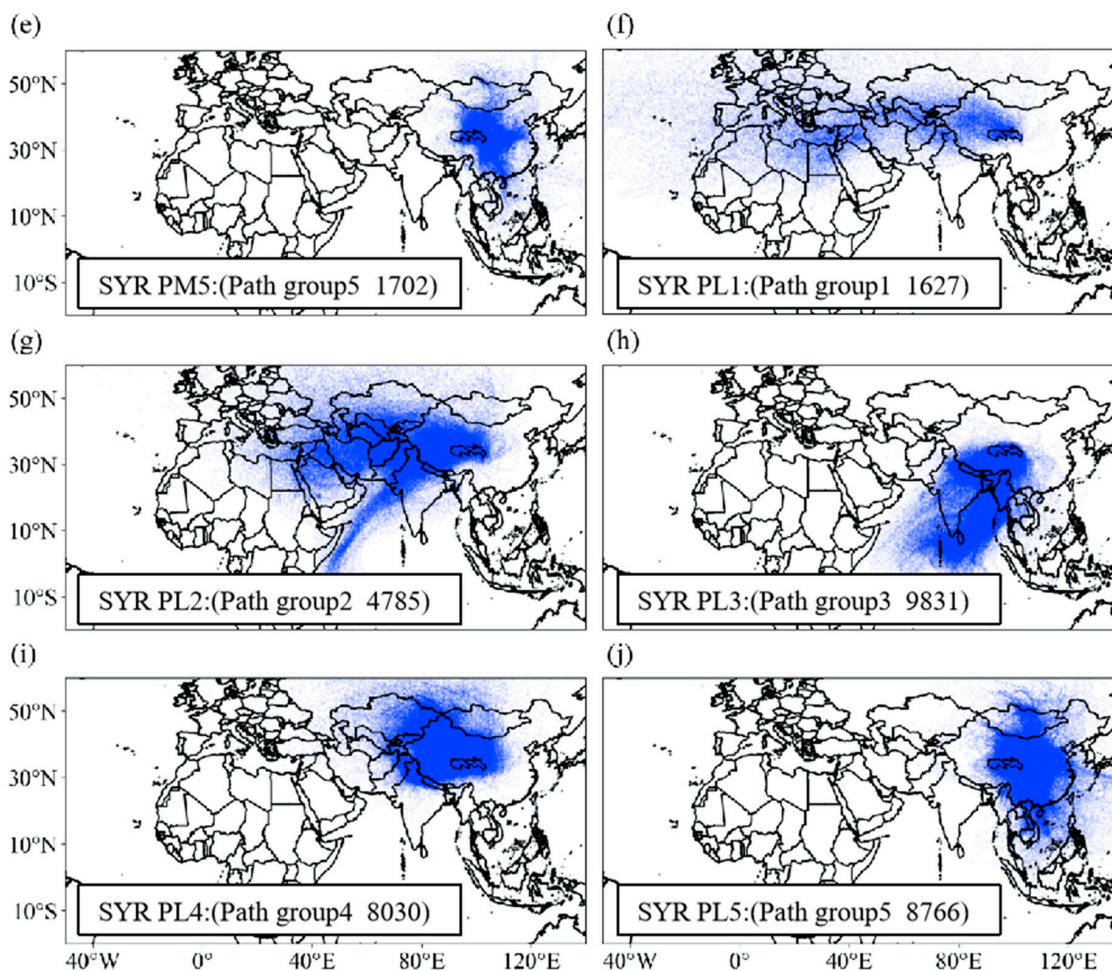


Figure 5. The clustering results of moisture trajectories for the SYR. The blue lines represent trajectories. (a–e) are PM events; (f–j) are PL events. PM indicates the daily precipitation is greater than 10 mm events; PL indicates the daily precipitation is less than 10 mm events. SYR indicates the source regions of the Yellow River basin. SYZR indicates the source regions of the Yangtze River basin.

3.2. Quantitative Importance of Major Moisture Transport Path Groups

Moisture undergoes multiple evaporation and precipitation losses during its transport, and specific humidity on the trajectories indicates changes in moisture content. The corresponding specific humidity changes along the paths of each cluster shown in Figures 6 and 7, indicate that many moisture paths undergo moisture losses before reaching the target region.

Overall, path group1 shows the most gradual humidity change, with lower specific humidity and the least contribution to precipitation in the river source regions. Path group3 exhibited the most drastic humidity changes, carrying a large amount of moisture from its origin and releasing a significant amount during transport. This path group contributed 2.5 times more to SYR precipitation than the SYZR. Path group2 has almost the same contribution rate to both river sources. Path group4 and path group5 show significant variations in moisture content along the trajectories.

Figure 6a–d for the SYZR during PM events in the last 6 h ($0 \sim -6$ h) show that the amount of moisture released by path group1, path group2, path group3, and path group4 is 90.7 , 305.4 , 870.8 , and $813.6 \text{ g}\cdot\text{kg}^{-1}(6 \text{ h})^{-1}$, respectively. These path groups contribute 4.36%, 14.68%, 41.87%, and 39.12%, respectively. Figure 6e–h during PL events for the SYZR in the last 6 h reveal that the amount of moisture released by path group1, path group2, path group3, and path group4 is 198.4 , 995.2 , 1930.1 , and $1548.5 \text{ g}\cdot\text{kg}^{-1}(6 \text{ h})^{-1}$, respectively. These path groups contributed 4.25%, 21.31%, 41.33%, and 33.16%, respectively.

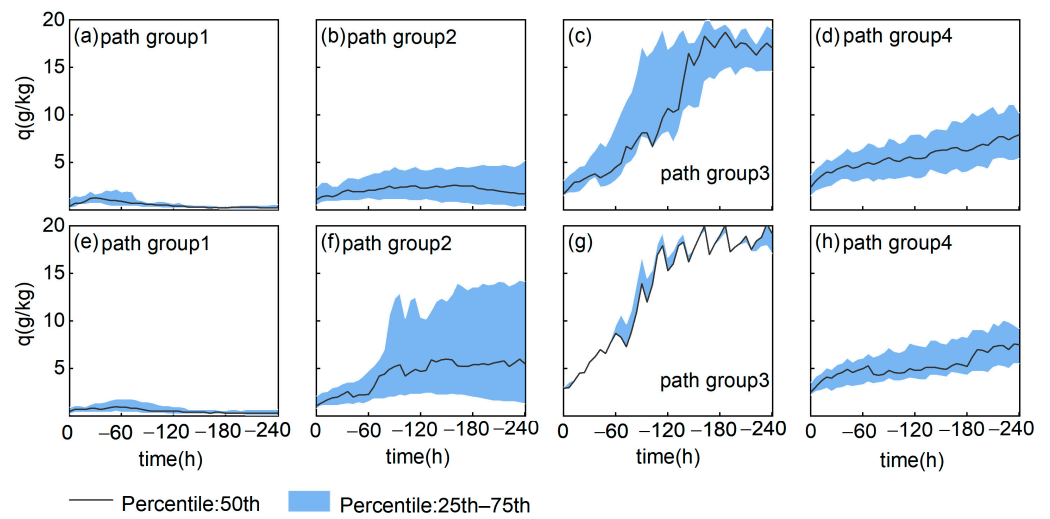


Figure 6. The specific humidity of different moisture path groups for the SYZR. (a–d) PM events of the SYZR; (e–h) PL events of the SYZR.

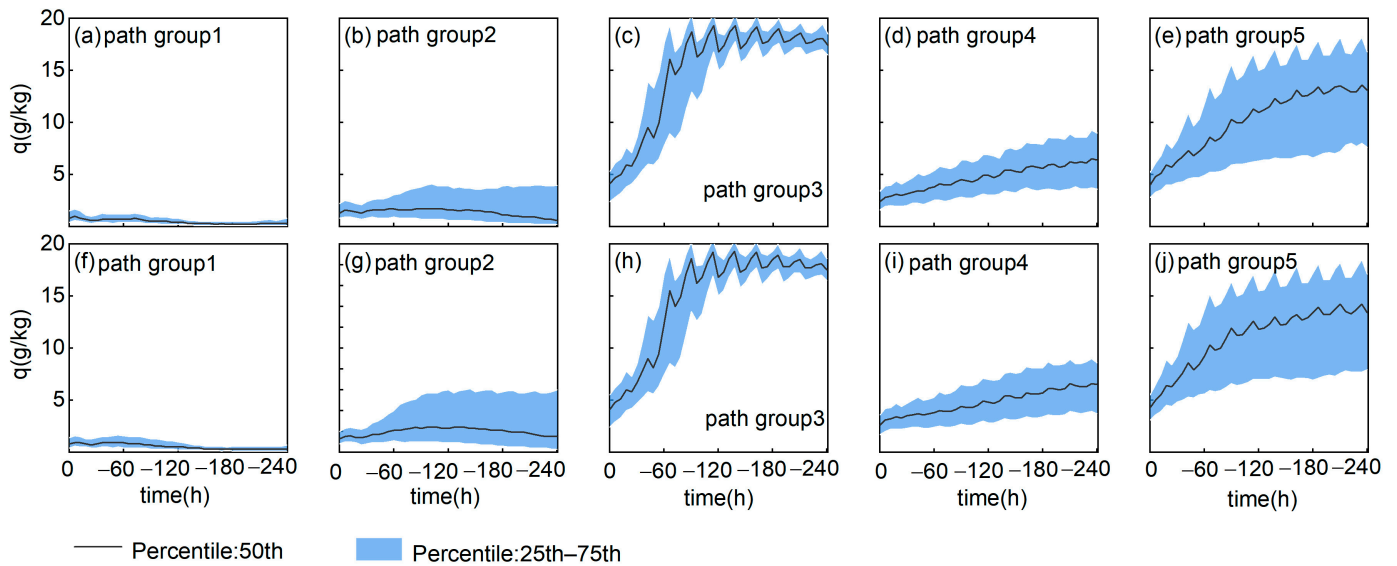


Figure 7. The specific humidity of different moisture path groups for the SYR. (a–e) PM events of the SYR; (f–j) PL events of the SYR.

For the SYR during PM events in the last 6 h as shown in Figure 7a–e, the amount of moisture released by path group1, path group2, path group3, path group4, and path group5 is 73.3, 312.5, 1050.7, 1145.8, and 941.5 $\text{g}\cdot\text{kg}^{-1}(6\text{ h})^{-1}$. These path groups contribute 2.08%, 8.87%, 29.83%, 32.53%, and 26.73%, respectively. Also, the amount of moisture released by path group1, path group2, path group3, path group4, and path group5 for the SYR during PL events in the last 6 h are shown in Figure 7f–j where 328.1, 1276.3, 6096.8, 6330.3, and 3470.5 $\text{g}\cdot\text{kg}^{-1}(6\text{ h})^{-1}$, respectively, were released. These path groups contributed 1.88%, 7.29%, 34.84%, 36.18%, and 19.83%, respectively.

In Figure 8, the total moisture released during PM and PL events for the SYZR was 2079.8 $\text{g}\cdot\text{kg}^{-1}(6\text{ h})^{-1}$ and 4669.8 $\text{g}\cdot\text{kg}^{-1}(6\text{ h})^{-1}$, respectively, while the total moisture released during PM and PL events for the SYR was 3522.0 $\text{g}\cdot\text{kg}^{-1}(6\text{ h})^{-1}$ and 17,497.6 $\text{g}\cdot\text{kg}^{-1}(6\text{ h})^{-1}$, respectively. The PL events of the SYR released a more significant amount of moisture, which was 3.7 times higher than that released by the PL events of the SYZR. The Bay of Bengal group, northwest China group, and southeast China group (path group3, 4, and 5) transported more moisture for the SYR.

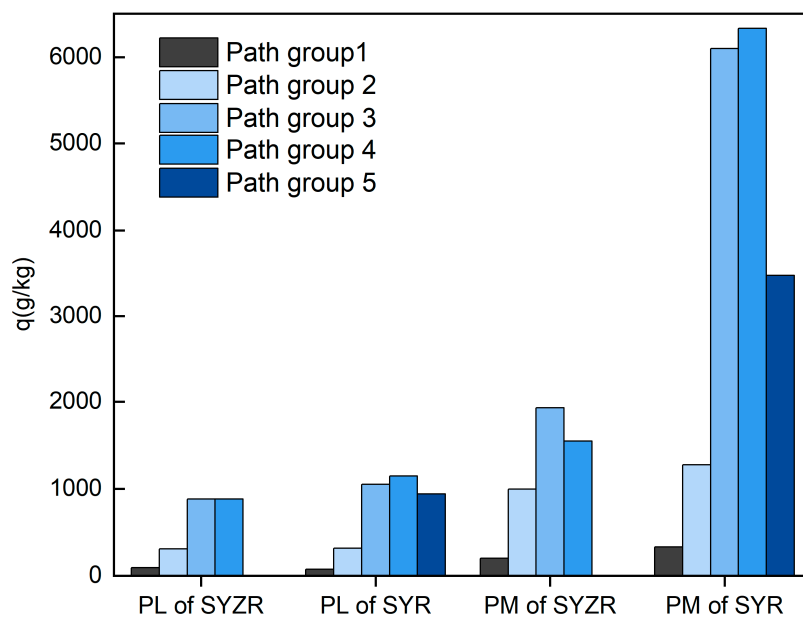


Figure 8. The amount of moisture released [$\text{g}\cdot\text{kg}^{-1}$] during different path groups in the last 6 h. PM of SYR indicates the PM events of the SYR. PL of SYR indicates the PL events of the SYR. PM of SYZR indicates the PM events of the SYZR. PL of SYZR indicates the PL events of the SYZR.

The statistical analysis of valid trajectories at different levels in the target region, as shown in Figure 9, reveals that the moisture release ($0 \sim -6$ h) heights in the river source regions are concentrated between 1500 and 2500 m above ground level (AGL). This altitude range is advantageous for conducting artificial weather modification operations.

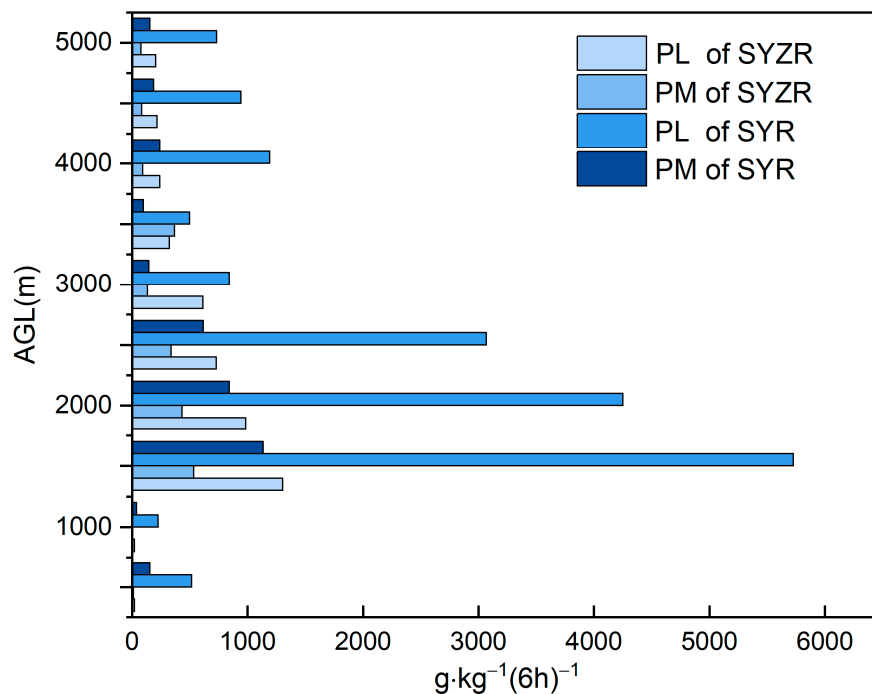


Figure 9. The amount of moisture released [g/kg] during different altitudes at the target region in the last 6 h. PM of SYR indicates the PM events of the SYR. PL of SYR indicates the PL events of the SYR. PM of SYZR indicates the PM events of the SYZR. PL of SYZR indicates the PL events of the SYZR.

3.3. Analysis of Moisture Exchange between the SYZR and SYR

The SYZR and SYR share valid trajectories that cross their respective borders because of their close proximities. Figure 10 presents results on the moisture exchange between the SYZR and SYR. During PM and PL events, the number of trajectories entering the SYZR from the SYR were 15 and 58, respectively, with a moisture release of about 7.1 g/kg and 16.30 g/kg. These values account for 0.34% and 0.35% of the total moisture release for the SYZR; these trajectories mainly belong to path group4 (northwest China group). Conversely, the number of trajectories entering the SYR from the SYZR were 798 and 3044 during the PM and PL events, with moisture releases of 257.4 g/kg and 1139.9 g/kg, constituting about 7.31% and 6.51% of its total moisture release, respectively; these trajectories mainly belong to path group3 (Bay of Bengal group), path group4 (northwest China group), and path group5 (southeast China group).

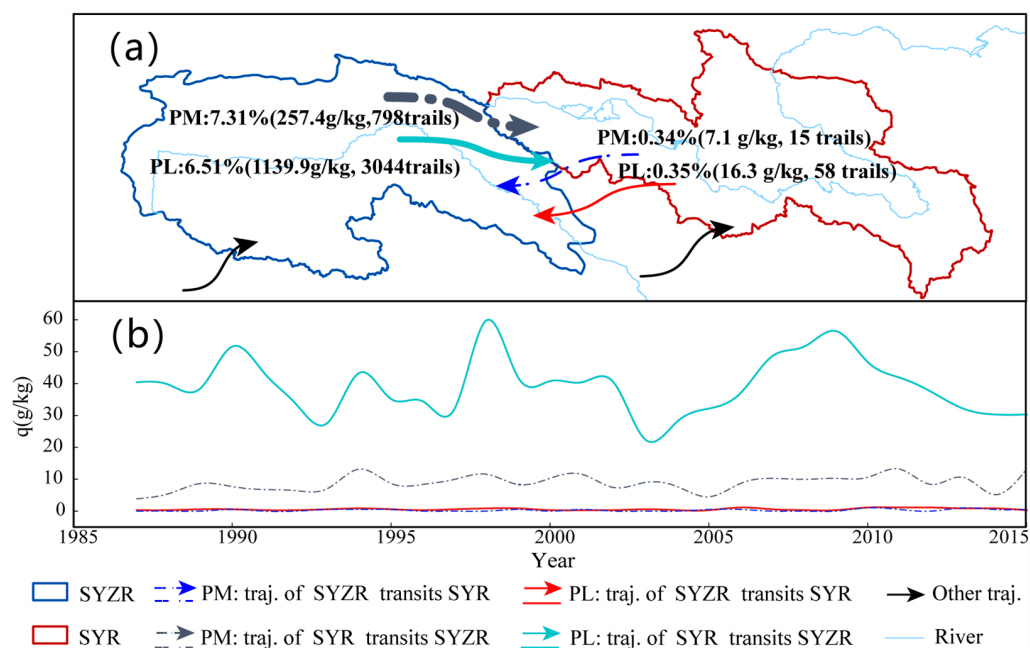


Figure 10. Moisture exchange between SYZR and SYR. (a) Total moisture exchange between SYZR and SYR from 1985 to 2015. (b) Annual variations in moisture exchange between SYZR and SYR.

The time series of the moisture exchange between the SYZR and SYR shows the annual summer moisture releases from the SYR to SYZR are close to zero but which from the SYZR to the SYR in PL events are about 39.26 g/kg (104.97 trajectories) and which from the SYZR to the SYR in PM events are about 8.84 g/kg (27.55 trajectories).

The attributed moisture release of each exchange trajectory between the SYZR and SYR is given in Figure 11. The moisture uptake locations belonging to each path group were divided into three categories: locations outside the source region of the two rivers (remote sources), locations inside the SYZR, and locations inside the SYR. For the PL events of the trajectories moving from the SYR to the SYZR, the moisture release of the four path groups is 1.37, 1.84, 0.28, and 9.34 $\text{g}\cdot\text{kg}^{-1}$ (240 h) $^{-1}$, respectively. Path group1, path group2, and path group3 are of limited importance (0.29‰, 0.40‰, 0.06‰), while path group4 plays a leading role (2.01‰). For the PM events of the trajectories moving from the SYR to the SYZR, the moisture release of the four path groups is 0.46, 0.29, 0.00, and 5.78 $\text{g}\cdot\text{kg}^{-1}$ (240 h) $^{-1}$, respectively. Path group1, path group2, and path group3 are of limited importance (0.22‰, 0.14‰, 0.00‰), while path group4 plays a leading role (2.77‰).

For the PL events of the trajectories moving from the SYZR to the SYR, the moisture release of the five path groups is 58.26, 54.58, 233.15, 242.48, and 344.56 $\text{g}\cdot\text{kg}^{-1}$ (240 h) $^{-1}$, respectively. Path group1 and path group2 are of limited importance (3.33‰, 3.12‰), while path group3, path group4, and path group5 play leading roles (13.32‰, 13.85‰, 19.68‰).

For the PM events of the trajectories moving from the SYZR to the SYR, the moisture release of the five path groups is 11.26, 109.73, 31.88¹, 49.13, and 11.25 g·kg⁻¹ (240 h)⁻¹, respectively. Path group1, path group3, and path group5 are of limited importance (3.12‰, 9.05‰, and 3.19‰), while path group2 and path group4 play leading roles (31.62‰ and 13.95‰).

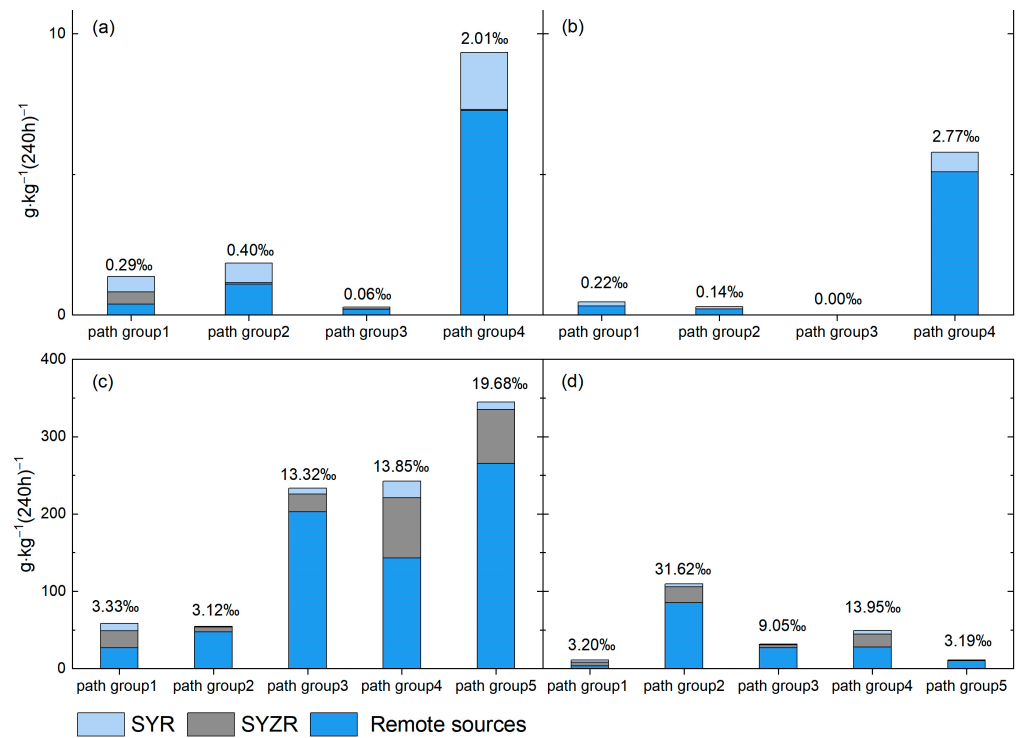


Figure 11. The amount of attributed moisture release [$\text{g}\cdot\text{kg}^{-1} (240\text{h})^{-1}$] by locations of each path group responsible for (a) trajectories to the SYZR that transit the SYR during PL events, (b) trajectories to the SYZR that transit the SYR during PM events, (c) trajectories to the SYR that transit the SYZR during PL events, and (d) trajectories to the SYR that transit the SYZR during PM events. The term “remote sources” refers to the aggregate moisture release attributed to regions beyond the moisture uptake locations in the source region of the two rivers. Bars in dark blue represent the amount of the attributed moisture release of remote sources’ moisture uptake locations, bars in gray represent the amount of the attributed moisture release of the SYR’s moisture uptake locations, and bars in light blue represent the amount of the attributed moisture release of the SYZR’s moisture uptake locations.

Given the higher proportion of trajectories from the SYZR entering the SYR, especially during the two events, it is crucial to analyze their trajectory frequency and average humidity (Figure 12). Its significant scientific and practical value of water resource security in the YR basin can be used for identifying the area where valid trajectories from the SYZR cross into the SYR.

The moisture paths’ frequencies of different precipitation types are shown in Figure 12a,b. During the PM events of the SYR, regions with a high frequency of trajectories crossing from the SYZR are found in the northernmost part of India. At the same time, those for the PL are primarily located along the southern foothills of the Himalayas, extending through Tibet to the target area. The trajectories entering the SYZR are concentrated along moisture transport path group2, 3, and 4 (nearer west group, Bay of Bengal group, northwest China group) of the SYZR. The high-frequency areas of SYR moisture crossing into the SYZR are located in the southeastern parts of Zhiduo County and Zaduo County.

Figure 12c,d show the mean specific humidity of moisture paths from the SYZR to the SYR for each grid cell. The average humidity of valid trajectories crossing from the SYZR into the SYR is lower in the TP, forming a band of low average humidity to the west of 34°

N latitude in the regions west of both the SYR and SYZR. Within the SYZR, the regions with a higher average humidity along the crossing trajectories are Chengdu County and Yushu City.

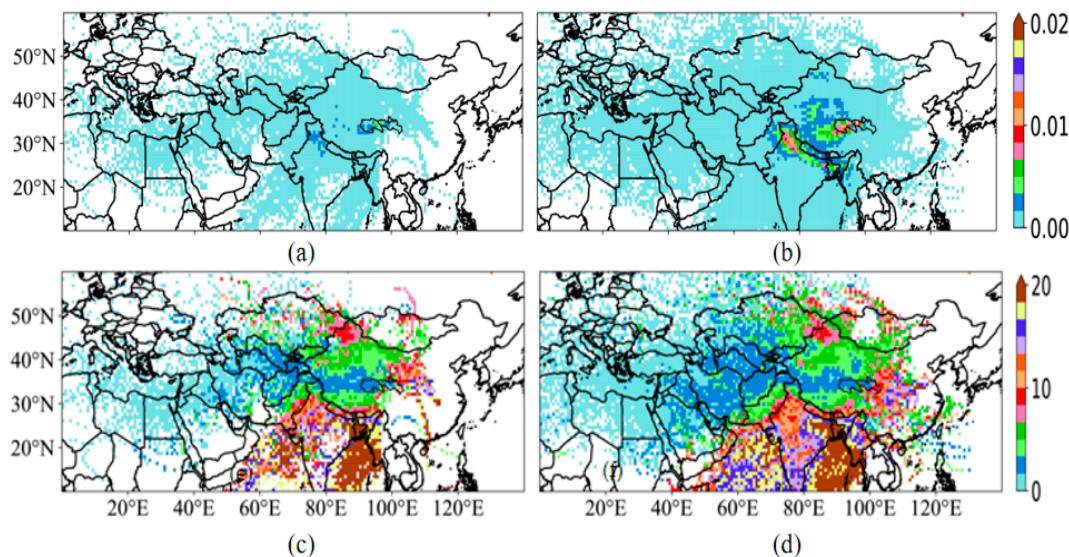


Figure 12. The frequency of the moisture paths (above) and mean specific humidity (g kg^{-1}) (below) from the SYZR to the SYR of moisture in (a,c) PM and (b,d) PL events.

The comparison reveals that although the areas with high trajectory frequency do not overlap with those of high average humidity, they are adjacent.

4. Conclusions and Discussion

4.1. Conclusions

This study investigates the major moisture transport pathways associated with two distinct types of daily precipitation occurrences (PM and PL events) throughout the summer in the SYZR and SYR regions. Additionally, it explores the characteristics of the reciprocal moisture exchange between the SYZR and the SYR.

The results of the moisture transport pathway identification suggest that path group3 (Bay of Bengal group) and path group4 (northwest China group) are the main and stable moisture transport pathways during PM and PL events in the SYZR [precipitation contribution: path group3, 41.87% (PM), 41.33% (PL); path group4, 39.12% (PM), 33.16% (PL)]. Path group3 (Bay of Bengal group), path group4 (northwest China group), and path group5 (southeast China group) are the main and stable moisture pathways during PM and PL events in the SYR [precipitation contribution: path group3, 29.83% (PM), 34.84% (PL); path group4, 32.53% (PM), 36.18% (PL); path group5, 26.73% (PM), 19.83% (PL)].

The amount of moisture transiting from the SYZR to the SYR was about 60 times that of the reverse, accounting for approximately 6.9% of the total precipitation moisture released in the SYR. The moisture pathways transiting from the SYZR to the SYR were present from 1986 to 2015. The amount of moisture through path group5 (southeast China group) from the SYZR to the SYR is relatively larger than other path groups during PL events. The amount of moisture through path group2 (nearer west group) from the SYZR to the SYR is relatively larger than other path groups during PM events. The areas with high trajectory frequency from the SYZR to the SYR were the southeast of Zhiduo County and the southeast of Zado County.

4.2. Discussion

Atmospheric water resources are abundant, such as a huge renewable reservoir [29]. This paper analyzed the characteristics of the moisture transport between the SYZR and

SYR, which is of great value to provide a full picture of the atmospheric hydrological cycle of the SYZR and SYR. There have been numerous experimental studies on the development of atmospheric water resources through artificial rain enhancement operations within the basin [30]. The study of moisture exchange between the SYZR and SYR provides a new perspective for the diversified development and utilization of atmospheric water resources in subsequent adjacent basins; this issue deserves a systematic and in-depth study.

As for the moisture pathways for the SYZR and SYR, there are already some studies on the moisture pathways of a related region. Yu Zhang et al. [13] noted that moisture paths from the northwest covering northwest China and Central Asia and moisture paths from southern and southeastern China are stable moisture transport pathways during extreme precipitation and moderate precipitation events over the TRHR of the TP. Nepiao Xu [12] noted that the climatological moisture sources over the TP were identified mainly at the southern and western boundaries, with the moisture sources at the southern boundaries originating from the Arabian Sea and Bay of Bengal and the moisture sources at the western boundary being transported by mid-latitude westerlies. Rong Liu [31] noted that the moisture pathways mainly came from the land and ocean in the west during the extreme drought episodes based on the standardized precipitation index (SPI). When the SPI indicated an extremely wet state, the transport mainly occurred to the east and south, including the Pacific Ocean and the South China Sea, where moisture entered the mainland from East/South China, passed through the Yangtze River basin, and finally reached the TRHR from the east or south of the TP. This is consistent with the view in this paper that the main moisture pathways are path group3 (Bay of Bengal group), path group4 (northwest China group), and path group5 (southeast China group).

The limitations of this study are that the K-means cluster results in the present study are relatively conservative; short paths tend to be grouped together as a clump with unclear directionality [such as path group1 (farther west group) and path group2 (nearer west group)], which is also noted by Borge et al. [32]. We think that this problem can be alleviated by introducing the direction of the previous part of the trajectories and consider it worthy of further efforts. Furthermore, the accuracy of the simulation results is influenced by various factors. Firstly, the influence of the data on simulation results is crucial. NOAA provides various data compatible with the HYSPLIT model, including NNR1, GDAS, and NCEP, among others. However, most studies rely on a single data source. For instance, Zhang et al. used NNR1 data to simulate the moisture trajectories of precipitation in the TRHR, while Xu et al. utilized ERA-interim data to simulate the moisture trajectories of precipitation in the Qinghai–Tibet Plateau. On the other hand, both Ayantobo et al. and our study employed NCEP data to simulate the moisture trajectories of precipitation. This reliance on a single data source may introduce biases in the results, and the reliability of the data is difficult to ascertain. Secondly, the settings for simulation altitude and starting time in the HYSPLIT model can also affect the accuracy of the results. Presently, most studies analyzing the characteristics of moisture transport simulate the moisture trajectories of daily precipitation events within the study area. Some studies only simulate trajectories at a single altitude on the day of precipitation, while others simulate trajectories at multiple altitudes on the day of precipitation, and still others simulate trajectories at multiple altitude levels until the end of the precipitation day. To refine the simulation, precipitation can be divided into events, and the starting point of the trajectory simulation can be set as the endpoint time of each precipitation event. This approach helps avoid inaccuracies in the choice of the simulation starting time. Additionally, the selection of simulation altitudes should consider the range of altitudes at which moisture is predominantly transported and should be based on the predominant distribution of moisture flux heights in the study area.

Through the analysis of moisture exchange characteristics between the two river source regions, it has been found that the moisture from the SYZR to the SYR accounts for 6.9% of the precipitation moisture in the SYR. Although the quantity is relatively small, it indicates the existence of a channel for moisture exchange. Regions such as Zhiduo County and the southeastern part of Zado County are characterized by high-frequency

trajectories of moisture exchange. In future research, advanced atmospheric simulation and prediction models, such as WRF, will be utilized to simulate artificial weather modification operations in key areas of moisture exchange (high-frequency trajectory regions) between the two river source regions. The impact on precipitation in the two river source regions will be evaluated. This will further analyze the feasibility of achieving the cross-basin allocation of atmospheric water resources and enhance the understanding of airborne water resource management.

Author Contributions: Conceptualization, J.W., B.K. and O.O.A.; methodology, J.W. and B.K.; software, B.K.; validation, J.W., B.K. and O.O.A.; formal analysis, J.W., B.K., H.Y. and O.O.A.; data curation, B.K.; writing—original draft preparation, B.K.; writing—review and editing, O.O.A., J.W., B.K. and H.Y.; project administration, J.W.; funding acquisition, J.W. All authors have read and agreed to the published version of the manuscript.

Funding: This research was funded by the National Natural Science Foundation of China, grant number U2243232; the Major Science and Technology Project of Qinghai Province, grant number 2021-SF-A6; and Qinghai University Young and Middle-aged Scientific Research Fund, grant number 2020-QGY-13.

Institutional Review Board Statement: Not applicable.

Informed Consent Statement: Not applicable.

Data Availability Statement: The data presented in this study are available on request from the corresponding author. The data are not publicly available due to approval process.

Conflicts of Interest: The authors declare no conflicts of interest.

Appendix A

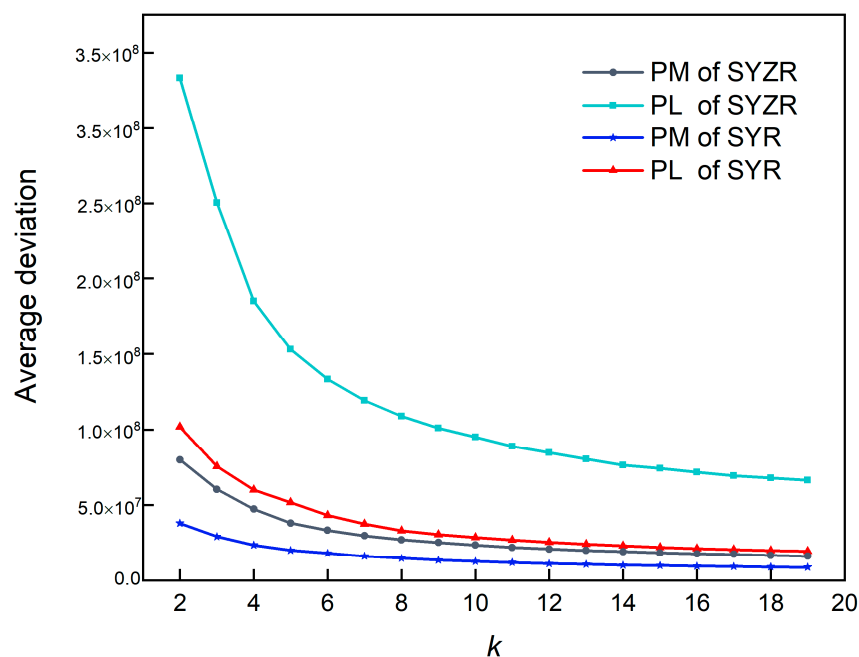


Figure A1. The average deviation for different numbers of clusters. PM of SYR indicates the PM events of the SYR. PL of SYR indicates the PL events of the SYR. PM of SYZR indicates the PM events of the SYZR. PL of SYZR indicates the PL events of the SYZR. PM indicates the daily precipitation is greater than 10 mm events; PL indicates the daily precipitation is less than 10 mm events. SYR indicates the source regions of the Yellow River basin. SYZR indicates the source regions of the Yangtze River basin. K indicates the clustering number.

Table A1. Silhouette coefficients for different numbers of clusters.

Region	Event	K = 2	K = 3	K = 4	K = 5	K = 6	K = 7	K = 8
SYZR	PM	0.513	0.295	0.320	0.313	0.313	0.311	0.314
	PL	0.587	0.410	0.433	0.427	0.461	0.472	0.477
SYR	PM	0.490	0.332	0.361	0.368	0.365	0.355	0.356
	PL	0.488	0.328	0.374	0.376	0.373	0.353	0.357

K indicates the clustering number.

References

- Wang, Y.; Ding, Y.; Ye, B.; Liu, F.; Wang, J.; Wang, J. Contributions of climate and human activities to changes in runoff of the Yellow and Yangtze rivers from 1950 to 2008. *Sci. China Earth Sci.* **2012**, *56*, 1398–1412. [CrossRef]
- Ayantobo, O.O.; Wei, J.; Shi, Y.; Wang, G. Climatological changes in rainfall distributions at different rain-rates under Qinghai-Tibet Plateau warming during 1981–2060. *Theor. Appl. Climatol.* **2023**, *152*, 663–679. [CrossRef]
- Wei, J. *A Research Report on Sanjiangyuanecological Protection: Volume of Hydrology and Water Resources*; Social Sciences Academic Press: Beijing, China, 2017; p. 2.
- Lu, W.; Wang, W.; Shao, Q.; Yu, Z.; Hao, Z.; Xing, W.; Yong, B.; Li, J. Hydrological projections of future climate change over the source region of Yellow River and Yangtze River in the Tibetan Plateau: A comprehensive assessment by coupling RegCM4 and VIC model. *Hydrol. Process.* **2018**, *32*, 2096–2117. [CrossRef]
- Cao, L.; Pan, S. Changes in precipitation extremes over the “Three-River Headwaters” region, hinterland of the Tibetan Plateau, during 1960–2012. *Quat. Int.* **2014**, *321*, 105–115. [CrossRef]
- Hu, Y.; Zhou, Y.; Wang, Y.; Lu, F.; Xiao, W.; Hou, B.; Yu, Y.; Liu, J.; Xue, W. Impacts of Precipitation Type Variations on Runoff Changes in the Source Regions of the Yangtze and Yellow River Basins in the Past 40 Years. *Water* **2022**, *14*, 4115. [CrossRef]
- Tang, Q.; Liu, Y.; Zhang, C.; Su, F.; Li, Y.; Gao, Y.; Li, W.; Chen, D. Research progress on moisture source change of precipitation over the Tibetan Plateau and its surrounding areas. *Trans. Atmos. Sci.* **2020**, *43*, 1002–1009. [CrossRef]
- Li, H.; Pan, X. An overview of research methods on water vapor transport and sources in the Tibetan Plateau. *Adv. Earth Sci.* **2022**, *37*, 1025–1036.
- Shi, X.; Shi, X. Climatic characteristics of water vapor budget over southeastern Tibetan Plateau in summer and their effects. *JAMS* **2008**, *19*, 41–46.
- Qiang, A.; Wang, N.; Xie, J.; Wei, J. Analysis of Water Vapor Change and Precipitation Conversion Efficiency Based on HYSPLIT Backward Trajectory Model over the Three-River Headwaters Region. *J. Coast. Res.* **2020**, *105*, 6–11. [CrossRef]
- Ayantobo, O.O.; Wei, J.; Hou, M.; Xu, J.; Wang, G. Characterizing potential sources and transport pathways of intense moisture during extreme precipitation events over the Tibetan Plateau. *J. Hydrol.* **2022**, *615*, 128734. [CrossRef]
- Xu, N.; Zhong, L.; Ma, Y.; Zou, M.; Huang, Z. A study on the water vapor transport trend and water vapor source of the Tibetan Plateau. *Theor. Appl. Climatol.* **2020**, *140*, 1031–1042. [CrossRef]
- Zhang, Y.; Huang, W.; Zhong, D. Major Moisture Pathways and Their Importance to Rainy Season Precipitation over the Sanjiangyuan Region of the Tibetan Plateau. *J. Clim.* **2019**, *32*, 6837–6857. [CrossRef]
- Tang, Q.; Zhang, C.; Chen, D. Recent Changes in the Moisture Source of Precipitation over the Tibetan Plateau. *J. Clim.* **2017**, *30*, 1807–1819. [CrossRef]
- Zhu, L.; Liu, R.; Wang, X.; Wang, Z.; Wen, J.; Zhao, Y.; Xie, Y.; Zhang, T. The characteristics of the water vapor transport and associated sources under abnormal precipitation conditions in the source region of the Yellow River using FLEXPART. *Plateau Meteorol.* **2019**, *38*, 484–496. [CrossRef]
- Li, J.; Li, T.; Wang, G.; Wei, J.; Zhong, D.; Su, Y.; Fu, X. Atmospheric water resource and precipitation conversion. *Chin. Sci. Bull.* **2018**, *63*, 2785–2796. [CrossRef]
- Ren, Z.H.; Zou, F.L.; Yu, Y.; Wang, G.A.; Zhang, Z.F.; Fan, S.H.; Zhang, Z.Q.; Sun, C. Dataset of Daily Climate Data from Chinese Surface Stations, Version 3.0. National Meteorological Information Center. Available online: <https://data.cma.cn/data/cdcindex/cid/f0fb4b55508804ca.html> (accessed on 5 January 2018).
- GB/T 28592-2012 *Grade of Precipitation*; General Administration of Quality Super Vision, Inspection and Quarantine of the People and Republic of China. Standards Press of China: Beijing, China, 2012.
- Yatagai, A.; Namiguchi, N.; Arakawa, O.; Hamada, A.; Yasutomi, N.; Nitoh, A. APHRODITE: Constructing a Long-Term Daily Gridded Precipitation Dataset for Asia Based on a Dense Network of Rain Gauges. *Bull. Am. Meteorol. Soc.* **2012**, *93*, 1401–1415. [CrossRef]
- Draxler, R.R.; Hess, G.D. *Description of the HYSPLIT_4 Modeling System*; NOAA Technical Memorandum ERL ARL-224; National Oceanic and Atmospheric Administration: Washington, DC, USA, 1997; 224p.
- Draxler, R.R.; Hess, G.D. An overview of the HYSPLIT_4 modelling system for trajectories, dispersion, and deposition. *Aust. Meteorol. Mag.* **1998**, *47*, 295–308.
- Wagner, T.; Andreae, M.O.; Beirle, S.; Dörner, S.; Mies, N.; Shaiganfar, R. MAX-DOAS observations of the total atmospheric water vapour column and comparison with independent observations. *Atmos. Meas. Tech.* **2013**, *6*, 131–149. [CrossRef]

23. Trenberth, N.E. Atmospheric Moisture Recycling: Role of Advection and Local Evaporation. *J. Clim.* **1999**, *12*, 1368–1381. [[CrossRef](#)]
24. Trenberth, N.E. Atmospheric Moisture Residence Times and Cycling: Implications for Rainfall Rates and Climate Change. *Clim. Chang.* **1998**, *39*, 667–694. [[CrossRef](#)]
25. Cohen, M.D.; Stunder, B.J.B.; Rolph, G.D.; Draxler, R.R.; Stein, A.F.; Ngan, F. NOAA's HYSPLIT Atmospheric Transport and Dispersion Modeling System. *Bull. Am. Meteorol. Soc.* **2015**, *96*, 2059–2077. [[CrossRef](#)]
26. Rousseeuw, P.J. Silhouettes: A graphical aid to the interpretation and validation of cluster analysis. *J. Comput. Appl. Math.* **1987**, *20*, 53–65. [[CrossRef](#)]
27. Sodemann, H.; Schwierz, C.; Wernli, H. Interannual variability of Greenland winter precipitation sources: Lagrangian moisture diagnostic and North Atlantic Oscillation influence. *J. Geophys. Res.* **2008**, *113*, D03107. [[CrossRef](#)]
28. Sun, B.; Wang, H. Moisture Sources of Semiarid Grassland in China Using the Lagrangian Particle Model FLEXPART. *J. Clim.* **2014**, *27*, 2457–2474. [[CrossRef](#)]
29. Wahlgren, R.V. Atmospheric water vapour processor designs for potable water production: A review. *Water Res* **2001**, *35*, 1–22. [[CrossRef](#)]
30. Flossmann, A.I.; Manton, M.; Abshaev, A.; Brintjes, R.; Murakami, M.; Prabhakaran, T.; Yao, Z. Review of Advances in Precipitation Enhancement Research. *Bull. Am. Meteorol. Soc.* **2019**, *100*, 1465–1480. [[CrossRef](#)]
31. Liu, R.; Wang, X.; Wang, Z. Atmospheric moisture sources of drought and wet events during 1979–2019 in the Three-River Source Region, Qinghai-Tibetan Plateau. *Theor. Appl. Climatol.* **2022**, *149*, 487–499. [[CrossRef](#)]
32. Borge, R.; Lumbreras, J.; Vardoulakis, S.; Nassomenos, P.; Rodriguez, E. Analysis of long-range transport influences on urban PM10 using two-stage atmospheric trajectory clusters. *Atmos. Environ.* **2007**, *41*, 4434–4450. [[CrossRef](#)]

Disclaimer/Publisher's Note: The statements, opinions and data contained in all publications are solely those of the individual author(s) and contributor(s) and not of MDPI and/or the editor(s). MDPI and/or the editor(s) disclaim responsibility for any injury to people or property resulting from any ideas, methods, instructions or products referred to in the content.